Pressure dependence of coherence-incoherence crossover behavior in KFe_{2}As_{2} observed by resistivity and ^{75}As-NMR/NQR

P. Wiecki, V. Taufour, D. Y. Chung, M. G. Kanatzidis, S. L. Bud'ko, P. C. Canfield, and Y. Furukawa

Phys. Rev. B **97**, 064509 — Published 13 February 2018

DOI: 10.1103/PhysRevB.97.064509

Pressure dependence of coherence-incoherence crossover behavior in KFe_2As_2 observed by resistivity and ^{75}As-NMR/NQR

P. Wiecki,[1] V. Taufour*,[1] D. Y. Chung,[2] M. G. Kanatzidis,[2,3] S. L. Bud'ko,[1] P. C. Canfield,[1] and Y. Furukawa[1]

[1] *Ames Laboratory, U.S. DOE and Department of Physics and Astronomy, Iowa State University, Ames, Iowa 50011 USA*
[2] *Materials Science Division, Argonne National Laboratory, Argonne, Illinois 60439, USA*
[3] *Department of Chemistry, Northwestern University, Evanston, Illinois 60208, USA*

(Dated: February 5, 2018)

We present the results of ^{75}As nuclear magnetic resonance (NMR), nuclear quadrupole resonance (NQR), and resistivity measurements in KFe_2As_2 under pressure (p). The temperature dependence of the NMR shift, nuclear spin-lattice relaxation time (T_1) and resistivity show a crossover between a high-temperature incoherent, local-moment behavior and a low-temperature coherent behavior at a crossover temperature (T^*). T^* is found to increase monotonically with pressure, consistent with increasing hybridization between localized 3d orbital-derived bands with the itinerant electron bands. No anomaly in T^* is seen at the critical pressure $p_c = 1.8$ GPa where a change of slope of the superconducting (SC) transition temperature $T_c(p)$ has been observed. In contrast, $T_c(p)$ seems to correlate with antiferromagnetic spin fluctuations in the normal state as measured by the NQR $1/T_1$ data, although such a correlation cannot be seen in the replacement effects of A in the AFe_2As_2 (A= K, Rb, Cs) family. In the superconducting state, two T_1 components are observed at low temperatures, suggesting the existence of two distinct local electronic environments. The temperature dependence of the short T_{1s} indicates nearly gapless state below T_c. On the other hand, the temperature dependence of the long component $1/T_{1L}$ implies a large reduction in the density of states at the Fermi level due to the SC gap formation. These results suggest a real-space modulation of the local SC gap structure in KFe_2As_2 under pressure.

PACS numbers:

I. I. INTRODUCTION

The iron-based superconductors (SCs) continue to be the focus of intense research in condensed matter physics, due to their unique interplay of magnetic, orbital and charge degrees of freedom[1–5]. Among the iron-based SCs, the heavily hole-doped iron-pnictide superconductor KFe_2As_2, with a SC transition temperature of $T_c \sim 3.5$ K, shows several unique properties. The Sommerfeld coefficient ($\gamma \sim 102$ mJ/molK^2) is significantly enhanced, and the magnetic susceptibility exhibits a broad peak around 100 K[6]. Nuclear magnetic resonance (NMR) spin-lattice relaxation rates ($1/T_1$) are strongly enhanced, evidencing antiferromagnetic spin fluctuations. Curie-Weiss fits to the NMR data have demonstrated the proximity of KFe_2As_2 to a quantum critical point (QCP)[7–9]. These results indicate a heavy quasiparticle effective mass and strong electronic correlations[6,7]. Recent NMR investigations have also pointed out the importance of ferromagnetic spin correlations in this material[7].

Furthermore, the SC properties of KFe_2As_2 are also unique. Whereas two full SC gaps are reported in the hole-doped series $Ba_{1-x}K_xFe_2As_2$ for $x < \sim 0.8$[10], a nodal SC gap structure in KFe_2As_2 ($x = 1$) has been suggested by several experiments[11–16]. A large full gap accompanied by several very small gaps has also been proposed based on specific heat measurements[17]. In addition, T_c shows non-monotonic behavior under pressure, with a minimum at $p_c \sim 1.8$ GPa, which has been suggested to be caused by a change in the SC gap structure[18–20]. Measurements of the pressure dependence of the upper critical field H_{c2} suggested the appearance of a k_z modulation of the SC gap above p_c[20].

Analogous behavior has also been found in the related alkali metal compounds $RbFe_2As_2$ and $CsFe_2As_2$[21–27], which show even greater mass enhancements with $\gamma \sim 127$ mJ/molK^2 and $\gamma \sim 184$ mJ/molK^2, respectively[28]. The unusual properties of the AFe_2As_2 (A = K, Rb, Cs) family have been pointed out[6,28,29] to be quite similar to f-electron heavy fermion materials[30,31], which display a crossover between a high-temperature incoherent, local-moment behavior and a low-temperature coherent behavior, with the crossover occurring at a temperature T^*. In this picture, the importance of dual role of Fe d electrons has been pointed out theoretically[32,33] where the two aspects of the itinerant and localized electrons may originate from different 3d orbitals of the iron ions. Recently, experimental[29,34] and theoretical[6] studies suggest that the bands derived from the Fe $3d_{xy}$ orbitals would play the role of the local moments. This orbital-selective localization is due to the strong Hund coupling in these materials[35].

Recent NMR measurements have pointed out a possible d-electron heavy fermion behavior in the AFe_2As_2 (A = K, Rb, Cs) family at ambient pressure[28]. T^* is reported to increase from 85 K for Cs, to 125 K for Rb

*Present address: Department of Physics, University of California, Davis, CA 95616, USA

and to 165 K for KFe_2As_2. Thermal expansion measurements on this family also find the lowest T^* for Cs and highest T^* for K, although the reported crossover temperatures are lower[36]. Since the so-called chemical pressure effects would increase when one moves from Cs to Rb to K due to the decrease in size of the alkali metal ion, this suggests that T^* increases with increasing the chemical pressure. Furthermore, two empirical relationships involving T^* have been discussed[28]. First, the superconducting transition temperature T_c is generally proportional to T^*, that is $T_c \propto T^*$, reflecting the correlation of T_c to local magnetic coupling J as pointed out in Ref. 37 in the context of f-electron heavy fermion SCs. Second, the Sommerfeld coefficient γ, and thus the effective mass m^*, is inversely proportional to T^*, that is $\gamma^{-1} \propto T^*$ (see also Ref. 6).

The $T_c \propto T^*$ relationship for the AFe_2As_2 (A = K, Rb, Cs) naively suggests that the non-monotonic behavior of T_c in these materials under pressure could be due to a non-monotonic behavior of T^* under pressure. This motivates an experimental investigation of the relationship between T_c and T^* under pressure. Here, we have carried out NMR and nuclear quadrupole resonance (NQR) measurements under high pressure up to 2.1 GPa and resistivity measurements up to ~ 5 GPa in order to investigate the pressure dependence of T^* and to test its relationship with T_c. Based on the NMR and resistivity data, we find that T^* increases monotonically with increasing pressure with no anomaly associated with crossing $p_c \sim 1.8$ GPa. These results indicate that T^* is not the primary driver of the pressure dependence of T_c in KFe_2As_2. On the other hand, $1/T_1$ measurements demonstrate that spin fluctuations are suppressed with increasing pressure up to the p_c and then start to be enhanced above p_c, suggesting that T_c is related to spin fluctuations in the normal state. In the superconducting state, two-component NQR relaxation is observed below $T = 1$ K, suggesting real space variation of the superconducting gap structure. One of the two components, the short T_1 component, shows no change in the slope of $1/T_1$ across T_c above 1.5 GPa, indicating these nuclei see a gapless local electronic environment in the SC state under these pressure conditions. Only the second component, the long T_1 component, shows a large reduction of the density of states at the Fermi energy due to the SC gap.

II. II. EXPERIMENTAL DETAILS

Highly pure KFe_2As_2 crystal sample was obtained by recrystallization of pre-reacted KFe_2As_2 polycrystalline powder in KAs flux as follows. KFe_2As_2 polycrystalline powder was prepared by annealing a stoichiometric mixture of K/Fe/As (0.27/0.77/1.03 g) contained in an alumina crucible which was subsequently sealed in a sealed silica tube under vacuum, at 700 °C for one day. KAs was prepared by heating a stoichiometric 1/1 ratio of K/As (0.94/1.80 g) in an alumina tube sealed in a silica tube at 250 °C for 12 h. The obtained KFe_2As_2 powder was then thoroughly mixed with KAs at a ratio of 1/4 (1.10/1.67 g) and heated to 1,050 °C for 12 h, followed by cooling slowly to room temperature at 5 °C/h. Isolation of KFe_2As_2 crystals from excess KAs flux was performed by dissolving KAs in ethanol for two days under nitrogen gas flow, which produces very shiny thin plate KFe_2As_2 crystals. The quality of KFe_2As_2 crystals was confirmed by a very sharp superconducting transition at 3.4 K from the magnetic susceptibility measurement.

^{75}As-NMR/NQR ($I = 3/2$; $\gamma/2\pi = 7.2919$ MHz/T; $Q = 0.29$ barns) measurements were performed using a lab-built, phase-coherent, spin-echo pulse spectrometer. The KFe_2As_2 sample was a fine powder in order to maximize the surface area for NMR/NQR measurements. The total mass of powder used in the high-pressure NMR/NQR measurements was ~ 15 mg. The ^{75}As-NMR spectra were obtained either by sweeping the magnetic field H at a fixed frequency $f = 54.8756$ MHz or by Fourier transform of the NMR echo signals at a constant magnetic field of $H = 7.41$ T. ^{75}As-NQR spectrum in zero field was measured in steps of frequency by measuring the intensity of the Hahn spin-echo. For our measurements at ultra-low temperatures below 1 K, we used a dilution refrigerator (Oxford Instruments, Kelvinox 100) where the pressure cell was mounted.

The ^{75}As NMR/NQR $1/T_1$ was measured with a recovery method using a single $\pi/2$ saturation pulse. For NMR measurements, the $1/T_1$ at each T was determined by fitting the nuclear magnetization m versus time t using the exponential function

$$1 - \frac{m(t)}{m(\infty)} = 0.1 \exp(-t/T_1) + 0.9 \exp(-6t/T_1), \quad (1)$$

where $m(t)$ and $m(\infty)$ are the nuclear magnetization at time t after the saturation and the equilibrium nuclear magnetization at $t \to \infty$, respectively. For NQR measurements, the recovery curve was fit to

$$1 - \frac{m(t)}{m(\infty)} = \exp(-3t/T_1). \quad (2)$$

Pressure was applied at room temperature using a hybrid CuBe/NiCrAl piston-cylinder-type high pressure clamp cell[38,39]. Daphne 7373 was chosen as the pressure transmitting medium. Pressure calibration was accomplished by ^{63}Cu-NQR in Cu_2O[40,41] at 77 K. In our pressure cell, the sample pressure decreases by $\sim$0.2 GPa when cooled from room temperature to 100 K, but remains constant below 100 K. The NMR coils inside the pressure cell consisted of $\sim$20 turns of 40AWG copper wire. The sample and calibration coils were oriented with their axes perpendicular to each other to avoid interference between coils.

The single-crystal electrical resistivity measurements were performed using the four-probe method with current in the ab plane[20]. Pressure was applied at room

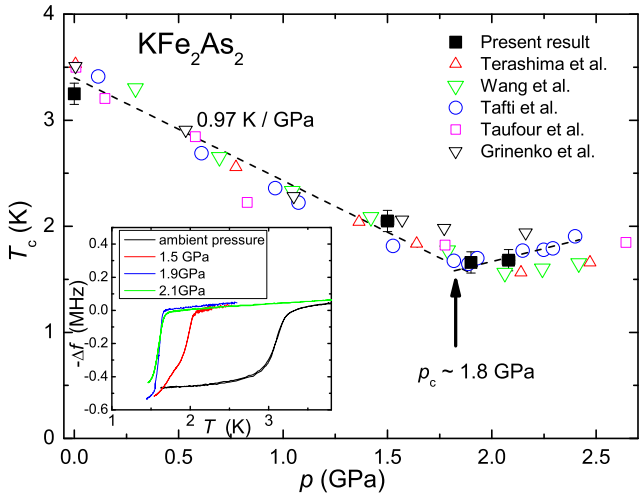

FIG. 1: Superconducting transition temperature T_c as a function of pressure determined by onset of Meissner effect measured by *in situ* ac-susceptibility. $p_c \sim 1.8$ GPa marks the critical pressure where T_c changes slope. Previously reported data are shown for comparison: Terashima *et al.* Ref. 19; Wang *et al.* Ref. 9; Tafti *et al.* Ref. 18; Taufour *et al.* Ref. 20; Grinenko *et al.* Ref. 43. Inset shows the typical temperature dependence of the change in the NMR coil tank circuit resonance frequency, Δf, under different pressures.

temperature using a modified Bridgman cell[42] with a 1:1 mixture of n-pentane:isopentane as a pressure medium, with the pressure determined using the superconducting transition of Pb.

III. III. RESULTS AND DISCUSSION

A. A. T_c and critical pressure

The superconducting transition temperature T_c of the KFe_2As_2 powder was determined by measuring the T dependence of the NMR coil tank circuit resonance frequency, $f(T)$, under zero magnetic field. The frequency f is a measure of the ac-susceptibility $\chi_{ac}(\omega_{NMR})$ since $f = 1/2\pi\sqrt{LC}$ and $L = L_0(1 + \chi_{ac})$. The onset of the Meissner effect therefore results in a sharp change of $f(T)$ as shown in the inset of Fig. 1. At ambient pressure, we find $T_c \sim 3.3$ K, as expected. The pressure dependence of T_c is shown in Fig. 1 together with the data reported previously[9,18–20,43,44]. T_c decreases with p below the critical pressure $p_c \sim 1.8$ GPa with a rate of 0.97 K/GPa, while T_c shows weak pressure dependence above p_c.

B. B. NMR spectrum

Figure 2 shows a representative field-swept NMR spectrum of the KFe_2As_2 powder measured at 10 K and $p = 1.9$ GPa. The spectrum is typical for an $I = 3/2$ nucleus in a powder sample with Zeeman interaction greater than quadrupole interaction. A central transition is flanked by two satellite lines split by the quadrupole interaction of the As nucleus with the local electric field gradient (EFG). In addition, the central transition line is split by the second-order quadrupole perturbation.

The situation is described by the spin Hamiltonian[45]

$$\mathcal{H} = -h\nu_L(1 + K_{z'})I_{z'} + \frac{h\nu_Q}{6}(3I_z^2 - I^2), \qquad (3)$$

appropriate for tetragonal crystals. Here z' is the direction of the applied field (H_{ext}) and z is the direction of the principal axis of the EFG. $\nu_L = \gamma H_{ext}/2\pi$ is the Larmor frequency and $K_{z'}$ represents the NMR shift. The quadrupole frequency for an $I = 3/2$ nucleus can be expressed as $\nu_Q = e^2QV_{zz}/2h$, e is the electron charge, Q is the nuclear quadrupole moment, V_{zz} is the EFG and h is Planck's constant. According to this Hamiltonian, the NMR spectrum depends on the angle θ between the external field and the EFG principal axis. To first order, the quadrupole satellite resonance frequencies are given by

$$\nu_\pm = \nu_L(1 + K_{z'}) \pm \frac{\nu_Q}{2}\left(3\cos^2\theta - 1\right) \qquad (4)$$

In second order perturbation theory, the central transition frequency depends on θ according to

$$\nu(\theta) = \nu_L\left(1 + K_{z'}\right) - \frac{3\nu_Q^2}{16\nu_L}\sin^2\theta(9\cos^2\theta - 1). \qquad (5)$$

In a powder sample, crystallites with all values of θ are present. Under these conditions the quadrupole satellites appear as sharp peaks at $\nu_L(1 + K_{z'}) \pm \nu_Q/2$ which correspond to $\theta = 90°$. For a powder, sharp peaks are observed in the central transition for $\theta = 90°$ and $\theta = \cos^{-1}(\sqrt{5/9}) = 41.8°$, as shown by the calculated powder-pattern spectrum in Fig. 2. The calculated spectrum assumes no preferential orientation of crystal grains, which is reasonable because the solidifications of the pressure medium prevent the crystal grains from reorienting. In a field-swept spectrum, the $\theta = 90°$ peak occurs at lower field, as indicated in Fig. 2. Since the EFG principal axis is along the c direction in KFe_2As_2, the $\theta = 90°$ peak arises from those crystallites that experience an external field in the crystal ab plane. We conducted our NMR shift and $1/T_1$ measurements at this peak of the central transition.

The quadrupole resonance frequency ν_Q was obtained by a direct measurement of the NQR spectrum at zero magnetic field. The typical NQR spectrum is shown in the inset of Fig. 3, where the full-width-at-half-maximum (FWHM) of the NQR spectrum is ~ 250 kHz at $T = 4.2$ K, which is consistent with the value reported previously[9] and is sharper than early NQR data measured at ambient pressure[11]. The temperature and pressure dependence of ν_Q is summarized in Fig. 3. As a function of temperature, ν_Q is nearly constant below 50 K, and increases slowly above 50 K, which is not simply explained

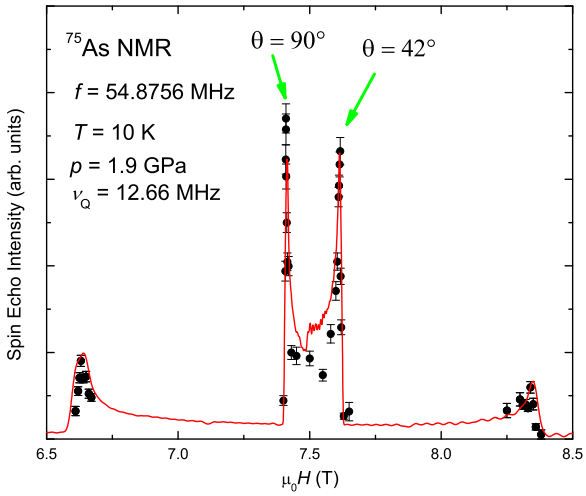

FIG. 2: Representative field-swept ^{75}As NMR spectrum of KFe_2As_2 powder measured at $T = 10$ K and $p = 1.9$ GPa. The central transition line is split into two lines by the second order quadrupole effect. θ is the angle between the external field and the principal axis of the electric field gradient (see text). The red curve is a simulated powder spectrum with $\nu_Q = 12.66$ MHz.

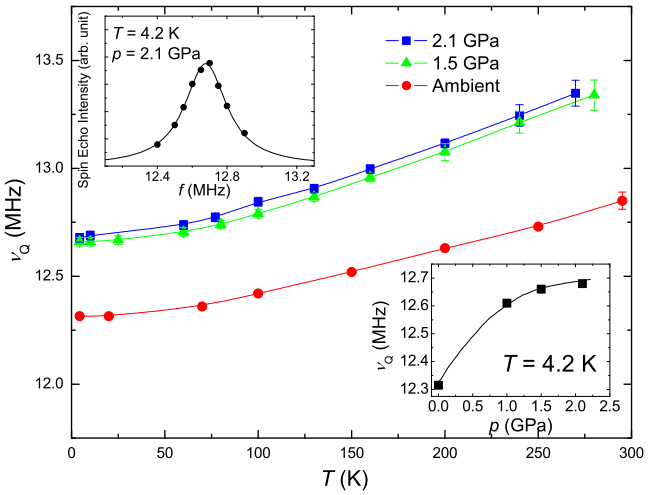

FIG. 3: Nuclear quadrupole resonance (NQR) frequency as a function of temperature for indicated pressures. Upper inset: Representative NQR spectrum at $p = 2.1$ GPa and $T = 4.2$ K, shown with a Lorentzian fit. Lower inset: NQR frequency as a function of pressure at $T = 4.2$ K. Lines are guides to the eye.

by the so-called $T^{3/2}$-law originating from the thermal vibrations of the lattice[46]. A similar increase of ν_Q at the Fe site is observed by Mössbauer measurements[47]. It is interesting to note that the value and temperature dependence of ν_Q in KFe_2As_2 is very similar to the ν_Q measured at the As(1) site near the K layer in the recently discovered superconductor $CaKFe_4As_4$, where magnetic fluctuations are involved to explain the temperature dependence[48]. As a function of pressure at constant temperature, ν_Q increases quickly up to 1.5 GPa, but increases slowly thereafter as in seen in the inset to Fig. 3. Similar pressure dependence of ν_Q in KFe_2As_2 has been reported[9]. No sharp anomalies are seen in ν_Q, indicating no structural phase transitions in the measured pressure and temperature range.

In order to precisely determine the NMR shift with external field applied in the ab plane, we performed Fourier transform measurements of the $\theta = 90°$ peak of the NMR central transition line at a constant magnetic field. In general, the central transition frequency is given by

$$\nu(\theta) = \nu_L \left(1 + \frac{2K_{\rm ab} + K_{\rm c}}{3}\right) + \frac{\nu_L}{3}(K_{\rm c} - K_{\rm ab})(3\cos^2\theta - 1) - \frac{3\nu_Q^2}{16\nu_L}\sin^2\theta(9\cos^2\theta - 1). \quad (6)$$

where $K_{\rm ab}$ and $K_{\rm c}$ are Knight shifts for $H \parallel ab$ plane and $H \parallel c$ axis, respectively. In the present case, since $\frac{3\nu_Q^2}{16\nu_L} \gg \frac{\nu_L}{3}(K_{\rm c} - K_{\rm ab})$ (Ref. 8 gives $|K_{\rm c} - K_{\rm ab}| \sim 0.001$), Eq. 6 can be simplified as

$$\nu(\theta = 90°) = \nu_L(1 + K_{\rm ab}) + \frac{3\nu_Q^2}{16\nu_L} \quad (7)$$

when $\theta = 90°$. We therefore obtain $K_{\rm ab}$ by subtracting $3\nu_Q^2/16\nu_L$ from the measured resonance frequency, $\nu(\theta = 90°)$.

The obtained NMR shifts are shown in Fig. 4. At ambient pressure, the NMR shift is nearly constant at low temperature and shows a broad peak near 150 K, before decreasing at high temperature. The behavior of $K_{\rm ab}$ is qualitatively similar under pressure, with the broad peak shifting to slightly higher temperature.

C. C. Crossover temperature T^*

The NMR shift data in Fig. 4 are consistent with a coherence/incoherence crossover behavior in KFe_2As_2 at all measured pressures. The broad peak in the NMR shift has been interpreted as the crossover from the high-temperature local-moment (Curie Weiss) behavior to the low temperature coherent state[6,28]. We could not reliably extract the crossover temperature T^* from the NMR shift data alone because of the weak temperature dependence of the NMR shift and also the broad quadrupole powder lineshape, although the data suggest a small increase of T^* under pressure.

The coherence/incoherence crossover temperature in KFe_2As_2 can also be estimated from the nuclear spin-lattice relaxation rate $1/T_1$ data, shown in Fig. 5. Our results for $1/T_1$ at ambient pressure are quantitatively consistent with Ref. 8. At low temperature, $1/T_1$ shows

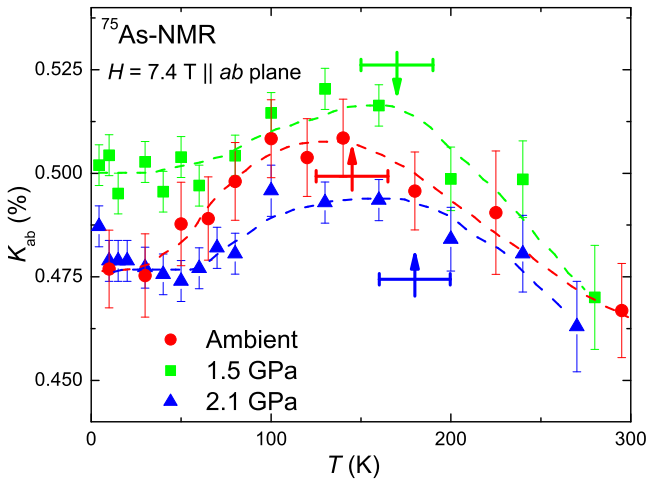

FIG. 4: NMR shift with external field aligned in the *ab* plane (K_{ab}) for indicated pressures. The dashed lines are guides to the eye. The arrows represent the crossover temperature T^*_{NMR} as determined by NMR $1/T_1$ measurements (see text and Fig. 5). The horizontal bars denote the uncertainty in estimation of T^*_{NMR} (±20 K).

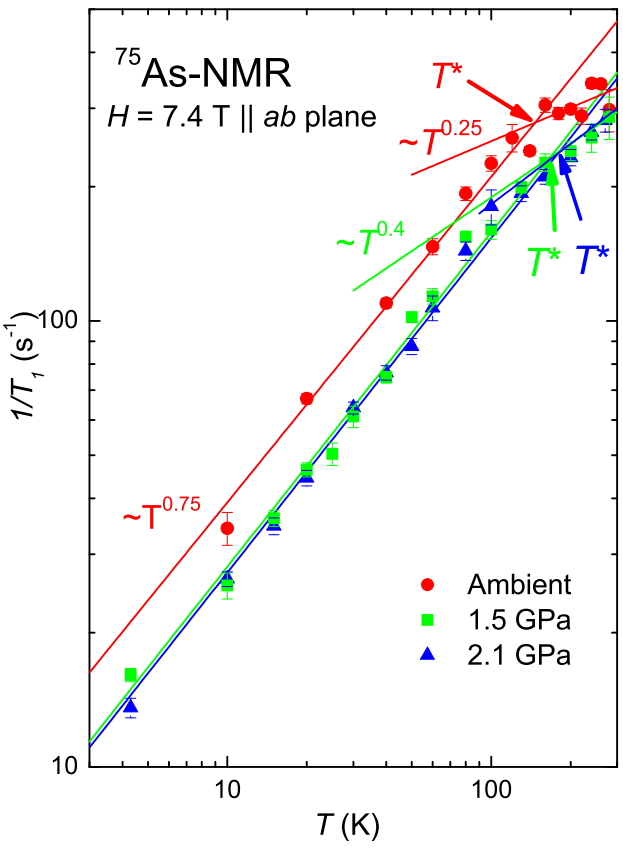

FIG. 5: NMR spin-lattice relaxation rate $1/T_1$ as a function of temperature. The coherence/incoherence crossover temperature T^*_{NMR} is found by the change of slope of $1/T_1$. The uncertainty in estimation of T^*_{NMR} is ±20 K (see text).

a power law behavior $1/T_1 \sim T^{0.75}$ for all pressures, as seen in Fig. 5. An obvious reduction in the slope of $1/T_1$ is seen at high temperature, however. Similar temperature dependence of $1/T_1$ is often observed in heavy fermion systems, where $1/T_1$ shows a power law behavior of $1/T_1 \propto T^{\alpha}$ (i.e. $\alpha = 0.25$ in $CeCoIn_5$[49] and $\alpha = 1$ in URu_2Si_2[50]) at low temperatures due to coherent metallic heavy fermion states and levels off at higher temperatures due to incoherent local moment behaviors. Thus the change in slope of the temperature dependence of $1/T_1$ gives an estimate of the coherence/incoherence crossover temperature (defined as T^*_{NMR}). From the T_1 data, we find $T^*_{NMR} \sim 145 \pm 20$ K at ambient pressure, $T^*_{NMR} \sim 170 \pm 20$ K at 1.5 GPa and $T^*_{NMR} \sim 180 \pm 20$ K at 2.1 GPa, indicating that T^*_{NMR} increases under pressure. The uncertainty in T^*_{NMR} is due primarily to uncertainty in the high-T slope (see below). These values of T^*_{NMR} seem to be consistent with the high-temperature end of the broad peak of K_{ab} (arrows in Fig. 4). The increase of T^*_{NMR} under pressure is reasonable, as the application of pressure should increase the hybridization between localized and itinerant electrons, thus increasing the local magnetic coupling J[37].

We also note that $1/T_1$ constant behavior above the coherent/incoherent crossover temperature T^* is observed in $CsFe_2As_2$[28], which has the highest effective mass of the AFe_2As_2 (A = K, Rb, Cs) family and therefore most localized electrons. However, as seen in Fig. 5, in KFe_2As_2 at ambient pressure $1/T_1$ does not level off completely above T^*_{NMR} but rather increases much more slowly, following roughly $1/T_1 \sim T^{0.25\pm0.1}$. Furthermore, as T^*_{NMR} increases under pressure, so does the slope of $1/T_1 \sim T^{0.4\pm0.1}$. It would be interesting if the high-temperature slope correlates with extent of the localization.

To corroborate our estimate of T^* and expand the results to pressures higher that those attainable in our NMR pressure cell, we also present and re-analyze single-crystal resistivity data up to ~ 5 GPa[20], as shown in Fig. 6(a). In heavy fermion systems, one expects a decrease of the resistivity below the coherence temperature, often showing a broad maximum at T^*[6,51]. While the NMR data provide incontrovertible evidence for coherence-incoherence crossover, the resistivity contains contributions from phonon scattering which complicate the interpretation of the data. The decrease in resistivity observed in Fig. 6(a) could, in principle, be due to the small Debye temperature and not electronic coherence effects. However, in the AFe_2As_2 (A = K, Rb, Cs) family, a strong correlation has been observed between T^*_{NMR} (as observed by NMR) and the cross point of two approximately linear trends in the resistivity[28]. This method, then, appears to give a reasonable estimate of T^* in these materials. Here we also apply this method to estimate T^* (defined as T^*_R) in KFe_2As_2 using the resistivity data. We note that our resistivity curves for different pressures can be scaled by a pressure depen-

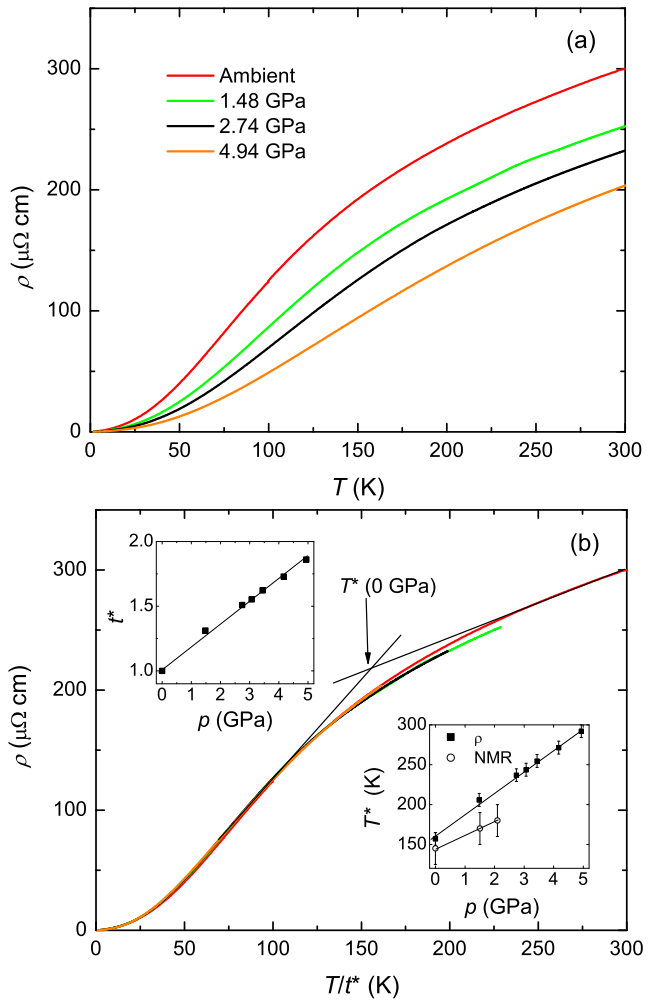

FIG. 6: (a) Resistivity of KFe_2As_2 single crystals[20] for selected pressures. (b) Resistivity plotted as a function of T/t^* where the scaling coefficient t^* is chosen so as to merge each curve with the ambient pressure curve. For ambient pressure, $t^* \equiv 1$. Upper inset: pressure dependence of the unitless scaling factor t^*. Lower inset: Comparison of pressure dependence of T^* as measured by resistivity (T^*_R; filled symbols) and NMR (T^*_{NMR}; open symbols). For resistivity $T^*_R = (157\ \mathrm{K})t^*$, where T^*_R at 0 GPa is determined by the crossing of two tangent lines, as proposed in Ref. 28 (see text).

dent scaling factor t^* (defined dimensionless), as shown in Fig. 6(b). The pressure dependence of t^* is shown in the upper inset. To estimate T^*_R from the resistivity data, we use the cross point of two approximately linear trends as shown in Fig. 6(b) where T^*_R is estimated to be $T^*_R = 157$ K for the ambient pressure data. Then, the pressure dependence of T^*_R can be obtained by using the pressure dependence of t^*. As shown in the lower inset of Fig. 6(b), T^*_R increases with increasing pressure. While the values of T^*_R extracted from the resistivity data up to 2.1 GPa are slightly higher than the T^*_{NMR} values identified by NMR data, both techniques show the increase of the coherent/incoherent crossover temperature T^* with applied pressure. It is clear that T^*_R evolves continuously, showing no anomaly at $p_c \sim 1.8$ GPa. It is interesting to note that the resistivity data for the Rb- and Cs-samples[28] can also be scaled to our ambient pressure data with $t^* = 0.78$ ($T^*_R = 123$ K) and $t^* = 0.52$ ($T^*_R = 82$ K) respectively.

We now consider the empirical relation that T_c is proportional to T^* observed in the AFe_2As_2 (A = K, Rb, Cs) family at ambient pressure[28]. Figure 7 plots our results for T_c as a function of T^* along with the results of Ref. 28. In the AFe_2As_2 (A= Cs, Rb, K) family at ambient pressure, T_c moves in proportion to T^*, suggesting that the change of T^* is the primary factor in determining T_c. In contrast, for pressurized KFe_2As_2 we find that T_c decreases sharply as a function of T^* below $p_c \sim 1.8$ GPa and then becomes roughly independent of T^* above p_c. These results indicate that T^* is not the primary driver of the pressure dependence of T_c in KFe_2As_2. Instead, as will be described in the next section, we show the antiferromagnetic spin fluctuations play an important role for the pressure dependence of T_c.

Finally, it is interesting to discuss the second empirical relation that $\gamma^{-1} \propto T^*$ under pressure. Quantum oscillation experiments under high pressure found that the effective mass m^* decreases under pressure[19]. In addition, the coefficient A in the low-temperature resistivity $\rho = \rho_0 + AT^2$ decreases smoothly, which is also consistent with a decreasing m^* under pressure[20]. The decreasing $m^* \sim \gamma$ accompanied by the increase of T^* suggest that the $\gamma^{-1} \propto T^*$ relationship seems to hold under pressure, similar to the case of AFe_2As_2 (A = K, Rb, Cs). As one moves from $CsFe_2As_2$ to $RbFe_2As_2$ to KFe_2As_2, the chemical pressure increases due to the decreasing size of the alkali metal ion[9]. Simultaneously, T^* increases[28]. Consequently, the increase of T^* in KFe_2As_2 under physical pressure could be considered an extension of the chemical pressure trend. However, it is noted that the $\gamma^{-1} \propto T^*$ relationship does not appear to hold the case of carrier doping in $Ba_{1-x}K_xFe_2As_2$ as seen in Ref. 36.

D. D. NQR Spin-Lattice Relaxation Rate

Since T^* evolves smoothly across the critical pressure p_c, the pressure dependence of the coherence/incoherence crossover behavior cannot explain the non-monotonic behavior of T_c under pressure in KFe_2As_2. To address this question, we have also performed NQR $1/T_1$ measurements in both the PM and SC states. No external magnetic field is required to measure NQR $1/T_1$, making this technique ideal for investigation of the SC state.

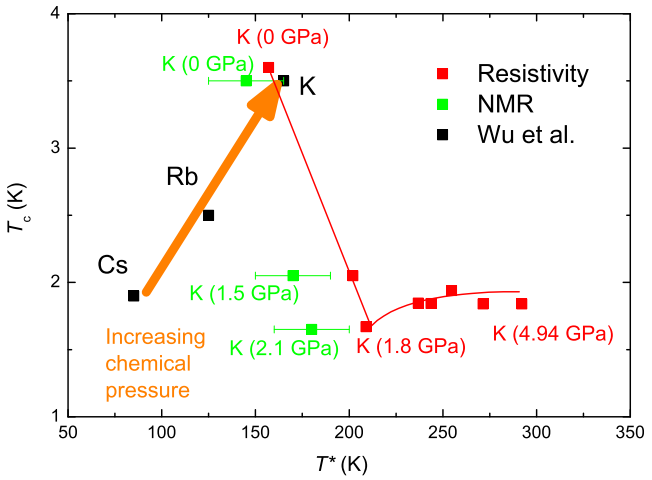

FIG. 7: Plot of T_c vs T^* for AFe_2As_2 (A = K, Rb, Cs) family at ambient pressure[28] (black). The orange arrow illustrates the increase of chemical pressure from $CsFe_2As_2$ to KFe_2As_2. The green data plots T_c vs T^* for KFe_2As_2 with indicated pressure as an implicit parameter, using T^*_{NMR} extracted from NMR measurements (see Fig. 5). Similarly, the red data shows T_c vs T^* for KFe_2As_2 using T^*_R extracted from resistivity measurements (see Fig. 6).

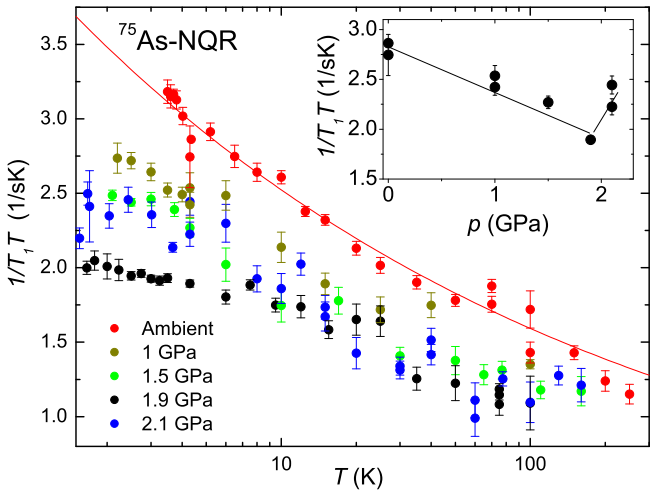

FIG. 8: NQR $1/T_1T$ above T_c for various pressures. The solid red curve for ambient pressure is a power law fit (see text). Inset: The value of NQR $1/T_1T$ at 4.2 K as a function of pressure.

1. 1. Paramagnetic State

First, we consider the NQR $1/T_1T$ in the PM state at ambient pressure. As seen in Fig. 8, the NQR $1/T_1T$ at ambient pressure follows a power law above T_c: $1/T_1 = 4T^{0.8} \Leftrightarrow 1/T_1T = 4T^{-0.2}$ (shown by the red solid curve in Fig. 8). This power law is consistent with previously reported NQR results at ambient pressure[11], and also NMR $1/T_1$ data ($1/T_1 \propto T^{0.75}$) described in the previous section. In general, the nuclear spin-lattice relaxation rate measures the $\mathbf{q}$-summed dynamical susceptibility at the Larmor frequency perpendicular to the quantization axis of nuclear spin,

$$\frac{1}{T_1T} \sim \gamma^2 k_B \sum_{\mathbf{q}} A_\perp^2(\mathbf{q}) \frac{\mathrm{Im}\chi_\perp(\mathbf{q},\omega_L)}{\omega_L}. \quad (8)$$

Therefore, since the NMR shift K, which reflects the $\mathbf{q} = 0$ component of χ, shows a weak temperature dependence, the increase of $1/T_1T$ at low temperatures reflects the enhancement of low-energy $\mathbf{q} \neq 0$ AFM spin fluctuations.

As shown in Fig. 8, the enhancements of $1/T_1T$ at low temperatures seems to be suppressed up to p_c and then starts to increase above p_c with increasing pressure, although the pressure dependence of $1/T_1T$ becomes less clear at high temperatures above ~ 10 K due to our experimental uncertainty. To see clearly the pressure dependence of low temperature $1/T_1T$ data, we plot the $1/T_1T$ values at 4.2 K as a function of pressure in the inset of Fig. 8. Here we took the $1/T_1T$ values at 4.2 K because enhancements of $1/T_1T$ due to the AF spin fluctuations are more significant at low temperatures and also the temperature is close to the lowest temperature above T_c in the paramagnetic state for all pressures measured. The value of $1/T_1T$ at 4.2 K clearly decreases with increasing pressure below p_c and then increases again above p_c. Since the value of $1/T_1T$ reflects the strength of low-energy AFM spin fluctuations, we conclude that spin fluctuations at low temperatures are suppressed below p_c and enhanced again above p_c. This trend is very similar to the pressure dependence of T_c. Therefore, we may conclude that AFM spin fluctuations are involved in the superconducting pairing both above and below p_c, consistent with the high-field NMR results[9].

However, it should be noted that the values of $1/T_1T$ decrease for the replacement of A from Cs to K in AFe_2As_2, despite the fact that T_c increases due to the replacement[28]. The relationship between T_c and $1/T_1$ therefore appears to be different in the pressure and replacement cases. Although at present the origin of the different behavior of T_c between the pressure and replacement cases is not understood well, we here discuss a few possibilities to explain the difference.

One possible difference between the pressure and replacement cases may relate to the anisotropy of magnetic fluctuations. According to Zhang *et al.*[52], based on their NMR data, the anisotropy of the low-temperature AFM fluctuations is found to significantly decrease with the replacement from Cs to K in AFe_2As_2. That is, the Cs sample with the lowest T_c in the family has the greatest anisotropy, suggesting that T_c may correlate with the anisotropy of the AFM fluctuations. Zhang *et al.* also suggested that the difference of the anisotropy may relate to quantum criticality and that the Cs sample is the closest to a QCP.

It is interesting to compare this to the behavior of the magnetic fluctuation anisotropy in KFe_2As_2 under pressure which can be obtained by taking a look at the ratio

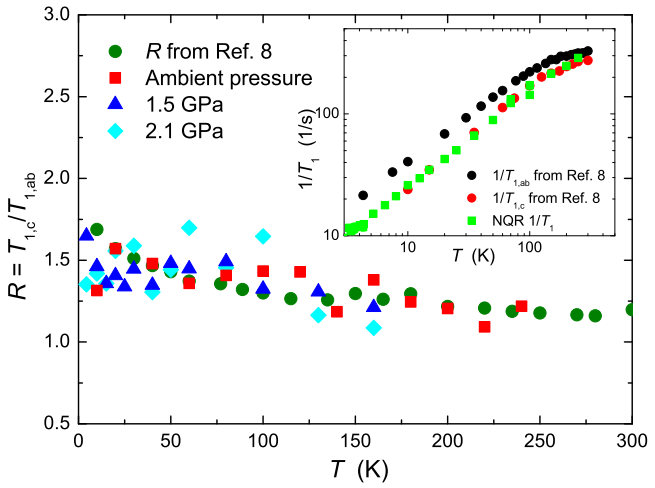

FIG. 9: T dependence of the ratio $R \equiv T_{1,c}/T_{1,ab}$ for different pressures where NQR-T_1 data are used for $T_{1,c}$, in addition to R obtained from $T_{1,c}/T_{1,ab}$ at ambient pressure from Ref. 8. NQR $1/T_1T$ above T_c for various pressures. The inset shows the T dependence of $1/T_1$ for $H||c$ and $H||ab$ from Ref. 8, together with NQR $1/T_1$ data.

of $1/T_1$ for the two field directions, $R \equiv (1/T_1)_{ab}/(1/T_1)_c$. According to the previous NMR studies performed on Fe pnictide SCs[8,53,54], the ratio R depends on the nature of magnetic fluctuations and also anisotropy of the magnetic fluctuations as

$$R = \begin{cases} 0.5 + \left(\frac{S_{ab}}{S_c}\right)^2 & \text{for the stripe AFM fluctuations} \\ 0.5 & \text{for the Néel-type spin fluctuations} \end{cases} \quad (9)$$

where $\mathcal{S}_\alpha$ is the amplitude of the spin fluctuation spectral density at NMR frequency along the α direction. Unfortunately, since we used a powder sample to improve the signal intensity, only $H||ab$ plane $1/T_1$ NMR measurements are feasible. Nevertheless, we can obtain some information about the anisotropy of the AFM spin fluctuations using our NQR $1/T_1$ data. Since the quantization axis of the electric field gradient is parallel to the c axis, the NQR $1/T_1$ should reflect magnetic fluctuations perpendicular to the c axis. These are the same fluctuations observed by NMR $1/T_1$ for $H||c$ axis, where the quantization axis is determined by the magnetic field. Indeed, we confirmed that our NQR $1/T_1$ data coincide almost perfectly with the NMR $1/T_1$ data under $H||c$ axis reported previously at ambient pressure[8], as shown in the inset of Fig. 9. This also indicates no magnetic field effects on $1/T_1$. Therefore, using both the NQR $1/T_1$ and NMR $1/T_1$ data under pressure, we can estimate how the anisotropy of magnetic fluctuations changes with pressure. The estimated R values using both the NQR $1/T_1$ and NMR $1/T_1$ data are shown in Fig. 9 as a function of temperature for different pressures. All R values are greater than unity, consistent with the stripe-type spin fluctuations. As shown, R does not show any significant change with pressure. This indicates that the anisotropy of spin fluctuations is almost independent of pressure, in contrast to the case of replacement effects on AFe_2As_2. We suggest that the different behaviors of the spin fluctuation anisotropy between the pressure and replacement cases may be related to the different behavior of T_c in the two cases. It is also interesting to note that several papers have proposed that, in the proximity of a QCP, the critical fluctuations may actually be detrimental to superconductivity in these systems[6,26,52]. Since $CsFe_2As_2$ is considered to be the closest to the QCP, it would be expected to have a low T_c.

It is also interesting to note in this context that in the hole-overdoped region of the $Ba_{1-x}K_xFe_2As_2$ phase diagram, the AFM spin fluctuations and Sommerfeld coefficient determined by specific heat measurements are both enhanced with increasing x while T_c decreases, similar to the case of AFe_2As_2 (A = K, Rb, Cs). One possible explanation for the decrease of T_c in $Ba_{1-x}K_xFe_2As_2$ is the growth of competing ferromagnetic (FM) spin fluctuations, which coexist with the AFM spin fluctuations[7]. As demonstrated by Wiecki *et al.*, the growth of the AFM fluctuations with increasing x in $Ba_{1-x}K_xFe_2As_2$ is accompanied by the simultaneous growth of FM fluctuations. These FM fluctuations may interfere with the AFM-fluctuation-based Cooper-pairing mechanism, thus lowering T_c despite the enhancement of AFM fluctuations. It is possible such physics could apply to the AFe_2As_2 (A=K, Rb, Cs) system also.

2. 2. Superconducting State

The T dependence of NQR $1/T_1$ below T_c is shown in Fig. 10. At ambient pressure, $1/T_1$ follows the power law $1/T_1 \sim T^{0.8}$ in the PM state as discussed above (red dashed line in Fig. 10). A clear kink is seen at T_c, and the data follow a new power law $1/T_1 \sim T^{1.3}$ below T_c (red solid line in Fig. 10). This behavior is consistent with previous ambient pressure NQR results[11]. However, in contrast to Ref. 11, a long T_1 component is found to appear below $T = 1$ K at ambient pressure and also under pressure. The upper inset of Fig. 10 shows the typical two-component exponential behavior of the nuclear magnetization recovery curve observed at low temperature ($T = 0.4$ K; $p = 1.5$ GPa), together with a single exponential behavior at $T = 3.73$ K and $p = 1.5$ GPa. Then, we fit the recovery curves according to

$$1 - \frac{m(t)}{m(\infty)} = A \exp\left(-3t/T_{1S}\right) + (1-A)\exp\left(-3t/T_{1L}\right), \quad (10)$$

where T_{1S} and T_{1L} are the short and long relaxation times, respectively. The parameter A, representing the fraction of nuclei relaxing with the shorter relaxation time T_{1S}, is shown in the lower inset of Fig. 10, demonstrating that the long T_{1L} component fraction increases with decreasing temperature.

The existence of two T_1 components implies the existence of two distinct local electronic environments, which

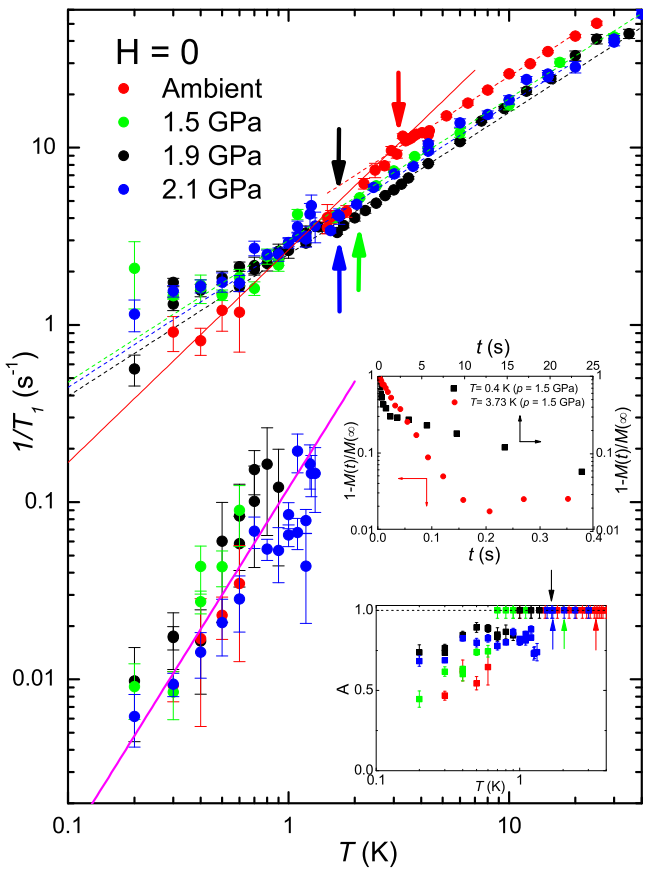

FIG. 10: NQR $1/T_1$ for indicated pressures. The arrows denote T_c at each pressure. The dashed lines are power law fits to the PM state data for each pressure. The red solid line below T_c shows the power law with $1/T_{1S} \propto T^{1.3}$ at ambient pressure. Below $T \sim 1$ K, a component with long T_1 appears. The solid pink line represents $1/T_{1L} \propto T^2$ behavior. Upper inset: The typical two exponential behavior (black squares) of the nuclear magnetization recovery curve observed at low temperature ($T = 0.4$ K; $p = 1.5$ GPa), together with a single exponential behavior (red circles) at $T = 3.73$ K and $p = 1.5$ GPa. Lower Inset: Fraction A of nuclei relaxing with the short T_1 (see text).

are physically separated in real space. Similar two-component relaxation has been observed by NQR in the closely-related sample $RbFe_2As_2$, in which the two-component behavior was argued to be associated with a charge order of nanoscale periodicity[27]. While we find no direct evidence for charge order in KFe_2As_2 in this study, charge ordering in KFe_2As_2 at 2.4 GPa (above our maximum pressure) was proposed by high pressure NMR[9]. Two-component relaxation has also been reported in $CsFe_2As_2$ under magnetic field in Refs. 28 (Supplemental Information), 29 and 55. At present, although the origin of the two T_1 components in KFe_2As_2 is not clear, the similar behavior in closely related systems would suggest that the two-component behavior observed here is intrinsic. Further studies will be needed to clarify the origin.

NQR $1/T_1$ is a sensitive probe of the reduction of the density of states (DOS) at the Fermi energy $N(E_F)$ due to the opening of the SC gap. In general, $1/T_1$ in the SC state is given by[56]

$$\frac{1}{T_1} \sim \int_0^\infty \left[N_s^2(E) + M_s^2(E)\right] f(E)(1 - f(E))\mathrm{d}E, \quad (11)$$

where $N_s(E)$ is the DOS and $f(E)$ is the Fermi distribution function. $M_s(E)$ is the anomalous DOS arising from Cooper pair coherence. Due to the lack of a coherence peak just below T_c, we neglect the coherence term, as has been done in previous NMR/NQR studies of FeAs superconductors.

The very weak decrease of the short component $1/T_{1S}$ below T_c ($1/T_{1S} \sim T^{1.3}$), implies a very small SC gap. Using a simple full gap model for $N_s(E)$, we estimate a gap of $\Delta(0) \sim 0.07$ meV ($2\Delta(0)/k_BT_c \sim 0.5$) from the short component, consistent with $2\Delta(0)/k_BT_c \sim 0.51$ reported by previous NQR measurements[11]. For all but the lowest temperatures measured, the relaxation is dominated by the short component, as shown by the inset of Fig. 10. This implies that a large number fraction of nuclei see a nearly gapless electronic environment below T_c. This may correspond to a large ungapped DOS below T_c in KFe_2As_2 observed by scanning tunneling spectroscopy (STS)[34]. The large ungapped DOS was attributed to a Van Hove singularity just below the Fermi level seen by angle resolved photoemission spectroscopy (ARPES)[34]. It is also worth mentioning that a residual DOS in SC state has been reported in $SrFe_2As_2$ under high pressure[57] and also in Co doped $BaFe_2As_2$ by specific heat measurements[58]. It is also suggested theoretically that the residual DOS is due to a possible formation of domain walls inherent to antiferromagnetism in iron pnicitde SCs[59].

In contrast, the long component $1/T_{1L}$ shows a large reduction relative to the $1/T_1$ in the PM state, implying a large reduction in $N_s(E_F)$ due to the SC gap. Although the experimental uncertainty is large, $1/T_{1L}$ seems to be proportional to $T^{2\pm1}$ as shown by the solid line in Fig. 10. The sizable depletion of $N_s(E_F)$ only below $T \sim 1$ K has been observed by the STS and ARPES experiments[34]. The co-existence of one large gap and at least one very small gap has also been reported with specific heat[17] and small angle neutron scattering[13] experiments. However, from the two-component relaxation behavior, our NQR data suggest a real-space modulation of the local gap structure, which has not been reported previously.

Under high pressure of 1.5 GPa and above, no obvious change of the slope of the short T_1 component occurs across T_c within our experimental uncertainty. This indicates that the nuclei relaxing according to $1/T_{1S}$ see a gapless local electronic environment above 1.5 GPa. Therefore the small gap seen by $1/T_{1S}$ at ambient pressure is thought to be suppressed to zero near p_c, and is not recovered above p_c. Similarly, muon spin rotation (μSR) measurements[60] on the closely-related $RbFe_2As_2$ with $p_c \sim 1.1$ GPa[24] reported that the smaller of two SC

gaps is suppressed to zero near 1 GPa. As for the long T_1 component under high pressure, as shown in Fig. 10, no obvious change in $1/T_{1L}$ can be found, suggesting no dramatic change in the magnitude of the larger SC gap upon pressure application. According to Ref. 20, the SC gap structure changes above p_c, where the SC gap is modulated along k_z. However, we did not observe a clear change in gap symmetry across p_c from our $1/T_1$ measurements.

IV. IV. CONCLUSIONS

We have presented ^{75}As-NMR, NQR and resistivity data which clearly show an increase of the coherence/incoherence crossover temperature T^* in KFe_2As_2 under pressure. This increase of T^* is expected due to the increase in hybridization between localized and conducting bands caused by pressure application. We find that the relation $\gamma^{-1} \sim T^*$ observed in ambient pressure AFe_2As_2 (A = K, Rb, Cs) continues to hold under pressure. However, the proportionality between T^* and T_c is clearly broken under pressure. The non-monotonic behavior of T_c under pressure is therefore unrelated to the coherence-incoherence crossover behavior in the paramagnetic state. However, the strength of AFM spin fluctuations in the paramagnetic state is found to correlate with T_c, evidencing clearly that the AFM spin fluctuations play an important role for the appearance of superconductivity in KFe_2As_2, although such a correlation cannot be seen in the replacement effects of A in the AFe_2As_2 (A= K, Rb, Cs) family. In the superconducting state, two T_1 components are observed at low temperatures, suggesting the existence of two distinct local electronic environments. The temperature dependence of the short T_{1s} indicates nearly gapless state below T_c. On the other hand, the temperature dependence of the long component $1/T_{1L}$ implies a large reduction in the density of states at the Fermi level due to the SC gap formation. These results suggest a real-space modulation of the local SC gap structure in KFe_2As_2 under pressure.

V. V. ACKNOWLEDGMENTS

We thank M. Tanatar for helpful discussions. The research was supported by the U.S. Department of Energy, Office of Basic Energy Sciences, Division of Materials Sciences and Engineering. Ames Laboratory is operated for the U.S. Department of Energy by Iowa State University under Contract No. DE-AC02-07CH11358. Work at Argonne National Laboratory was supported by the U.S. Department of Energy, Office of Science, Basic Energy Sciences under Contract No. DE-AC02-06CH11357.

[1] P. C. Canfield and S. L. Bud'ko, Annu. Rev. Condens. Matter Phys. **1**, 27 (2010).
[2] D. C. Johnston, Adv. Phys. **59**, 803 (2010).
[3] R. M. Fernandes, A. V. Chubukov, and J. Schmalian, Nat. Phys. **10** 97 (2014).
[4] Q. Si, R. Yu, and E. Abrahams, Nat. Rev. Mats. **1**, 16017 (2016). doi:10.1038/natrevmats.2016.17
[5] P. Dai, Rev. Mod. Phys. **87** 855 (2015).
[6] F. Hardy, A. E. Böhmer, D. Aoki, P. Burger, T. Wolf, P. Schweiss, R. Heid, P. Adelmann, Y. X. Yao, G. Kotliar, J. Schmalian, and C. Meingast Phys. Rev. Lett. **111**, 027002 (2013).
[7] P. Wiecki, B. Roy, D. C. Johnston, S. L. Bud'ko, P. C. Canfield, and Y. Furukawa, Phys. Rev. Lett. **115**, 137001 (2015).
[8] M. Hirano, Y. Yamada, T. Saito, R. Nagashima, T. Konishi, T. Toriyama, Y. Ohta, H. Fukazawa, Y. Kohori, Y. Furukawa, K. Kihou, C.-H. Lee, A. Iyo, H. Eisaki, J. Phys. Soc. Jpn., 81, 054704 (2012).
[9] P. S. Wang, P. Zhou, J. Dai, J. Zhang, X. X. Ding, H. Lin, H. H. Wen, B. Normand, R. Yu, and W. Yu, Phys. Rev. B **93**, 085129 (2016).
[10] H. Ding, P. Richard, K. Nakayama, K. Sugawara, T. Arakane, Y. Sekiba, A. Takayama, S. Souma, T. Sato, T. Takahashi, Z. Wang, X. Dai, Z. Fang, G. F. Chen, J. L. Luo, and N. L. Wang, Europhys. Lett. **83** 47001 (2008).
[11] H. Fukazawa, Y. Yamada, K. Kondo, T. Saito, Y. Kohori, K. Kuga, Y. Matsumoto, S. Nakatsuji, H. Kito, P. M. Shirage, K. Kihou, N. Takeshita, C.-H. Lee, A. Iyo, and H. Eisaki, J. Phys. Soc. Jpn. **78**, 083712 (2009).
[12] K. Hashimoto, A. Serafin, S. Tonegawa, R. Katsumata, R. Okazaki, T. Saito, H. Fukazawa, Y. Kohori, K. Kihou, C. H. Lee, A. Iyo, H. Eisaki, H. Ikeda, Y. Matsuda, A. Carrington, and T. Shibauchi, Phys. Rev. B **82**, 014526 (2010).
[13] H. Kawano-Furukawa, C. J. Bowell, J. S. White, R. W. Heslop, A. S. Cameron, E. M. Forgan, K. Kihou, C. H. Lee, A. Iyo, H. Eisaki, T. Saito, H. Fukazawa, Y. Kohori, R. Cubitt, C. D. Dewhurst, J. L. Gavilano, and M. Zolliker, Phys. Rev. B **84**, 024507 (2011).
[14] J. P. Reid, M. A. Tanatar, A. Juneau-Fecteau, R. T. Gordon, S. R. de Cotret, N. Doiron-Leyraud, T. Saito, H. Fukazawa, Y. Kohori, K. Kihou, C. H. Lee, A. Iyo, H. Eisaki, R. Prozorov, and L. Taillefer, Phys. Rev. Lett. **109**, 087001 (2012).
[15] K. Okazaki, Y. Ota, Y. Kotani, W. Malaeb, Y. Ishida, T. Shimojima, T. Kiss, S. Watanabe, C. T. Chen, K. Kihou, C. H. Lee, A. Iyo, H. Eisaki, T. Saito, H. Fukazawa, Y. Kohori, K. Hashimoto, T. Shibauchi, Y. Matsuda, H. Ikeda, H. Miyahara, R. Arita, A. Chainani, and S. Shin, Science **337**, 1314 (2012).
[16] Y. Ota, K. Okazaki, Y. Kotani, T. Shimojima, W. Malaeb, S. Watanabe, C.-T. Chen, K. Kihou, C. H. Lee, A. Iyo, H. Eisaki, T. Saito, H. Fukazawa, Y. Kohori, and S. Shin Phys. Rev. B **89**, 081103(R) (2014).
[17] F. Hardy, R. Eder, M. Jackson, D. Aoki, C. Paulsen, T. Wolf, P. Burger, A. Böhmer, P. Schweiss, P. Adelmann, R. A. Fisher, and C. Meingast, J. Phys. Soc. Jpn. **83** 014711 (2014).
[18] F. F. Tafti, A. Juneau-Fecteau, M.-E. Delage, S. R. de

Cotret, J.-P. Reid, A. F. Wang, X.-G. Luo, X. H. Chen, N. Doiron-Leyraud, and L. Taillefer, Nat. Phys. **9**, 349 (2013).
[19] T. Terashima, K. Kihou, K. Sugii, N. Kikugawa, T. Matsumoto, S. Ishida, C.-H. Lee, A. Iyo, H. Eisaki, and S. Uji, Phys. Rev. B **89**, 134520 (2014).
[20] V. Taufour, N. Foroozani, M. A. Tanatar, J. Lim, U. Kaluarachchi, S. K. Kim, Y. Liu, T. A. Lograsso, V. G. Kogan, R. Prozorov, S. L. Bud'ko, J. S. Schilling, and P. C. Canfield Phys. Rev. B **89**, 220509(R) (2014).
[21] X. C. Hong, X. L. Li, B. Y. Pan, L. P. He, A. F. Wang, X. G. Luo, X. H. Chen, and S. Y. Li, Phys. Rev. B **87**, 144502 (2013).
[22] F. F. Tafti, J. P. Clancy, M. Lapointe-Major, C. Collignon, S. Faucher, J. A. Sears, A. Juneau-Fecteau, N. Doiron-Leyraud, A. F. Wang, X.-G. Luo, X. H. Chen, S. Desgreniers, Y.-J. Kim, and L. Taillefer, Phys. Rev. B **89**, 134502 (2014).
[23] Z. Zhang, A. F. Wang, X. C. Hong, J. Zhang, B. Y. Pan, J. Pan, Y. Xu, X. G. Luo, X. H. Chen, and S. Y. Li, Phys. Rev. B **91**, 024502 (2015).
[24] F. F. Tafti, A. Ouellet, A. Juneau-Fecteau, S. Faucher, M. Lapointe-Major, N. Doiron-Leyraud, A. F. Wang, X.-G. Luo, X. H. Chen, and L. Taillefer, Phys. Rev. B **91**, 054511 (2015).
[25] Y. Mizukami, Y. Kawamoto, Y. Shimoyama, S. Kurata, H. Ikeda, T. Wolf, D. A. Zocco, K. Grube, H. v. Löhneysen, Y. Matsuda, and T. Shibauchi Phys. Rev. B **94**, 024508 (2016).
[26] F. Eilers, K. Grube, D. A. Zocco, T. Wolf, M. Merz, P. Schweiss, R. Heid, R. Eder, R. Yu, J.-X. Zhu, Q. Si, T. Shibauchi, and H. v. Löhneysen, Phys. Rev. Lett. **116**, 237003 (2016).
[27] E. Civardi, M. Moroni, M. Babij, Z. Bukowski, and P. Carretta, Phys. Rev. Lett. **117**, 217001 (2016).
[28] Y. P. Wu, D. Zhao, A. F. Wang, N. Z. Wang, Z. J. Xiang, X. G. Luo, T. Wu, and X. H. Chen, Phys. Rev. Lett. **116**, 147001 (2016).
[29] D. Zhao, S. J. Li, N. Z. Wang, J. Li, D. W. Song, L. X.Zheng, L. P. Nie, X. G. Luo, T. Wu, X. H. Chen, arXiv:1705.09885 [cond-mat.supr-con].
[30] P. Gegenwart, Q. Si, F. Steglich, Nat. Phys. **4** 186 (2008).
[31] N. J. Curro, Rep. Prog. Phys. **72** 026502 (2009).
[32] Y.-Z. You, F. Yang, S.-P. Kou, and Z.-Y. Weng, Phys. Rev. B **84**, 054527 (2011).
[33] L. P. Gor'kov and G. B. Teitel'baum, Phys. Rev. B **87**, 024504 (2013).
[34] D. Fang, X. Shi, Z. Du, P. Richard, H. Yang, X. X. Wu, P. Zhang, T. Qian, X. Ding, Z. Wang, T. K. Kim, M. Hoesch, A. Wang, X. Chen, J. Hu, H. Ding, and H.-H. Wen, Phys. Rev. B **92**, 144513 (2015).
[35] A. Georges, L. de' Medici, and J. Mravlje, Annu. Rev. Condens. Matter Phys. **4** 137 (2013).
[36] F. Hardy, A. E. Böhmer, L. de' Medici, M. Capone, G. Giovannetti, R. Eder, L. Wang, M. He, T. Wolf, P. Schweiss, R. Heid, A. Herbig, P. Adelmann, R. A. Fisher, and C. Meingast, Phys. Rev. B **94**, 205113 (2016).
[37] D. Pines, J. Phys. Chem. B 117, 13145 (2013).
[38] N. Fujiwara, T. Matsumoto, K. Koyama-Nakazawa, A. Hisada and Y. Uwatoko, Rev. Sci. Instrum. **78**, 073905 (2007).
[39] N. Aso, T. Fujiwara, Y. Uwatoko, H. Miyano, H. Yoshizawa, J. Phys. Soc. Jpn. **76** Suppl. A, pp. 228-229 (2007).
[40] H. Fukazawa, N. Yamatoji, Y. Kohori, C. Terakura, N. Takeshita, Y. Tokura and H. Takagi, Rev. Sci. Instrum. **78**, 015106 (2007).
[41] A. P. Reyes, E. T. Ahrens, R. H. Heffner, P. C. Hammel, and J. D. Thompson, Rev. Sci. Instrum. **63**, 3120 (1992).
[42] E. Colombier and D. Braithwaite, Rev. Sci. Instrum. **78**, 093903 (2007).
[43] V. Grinenko, W. Schottenhamel, A. U. B. Wolter, D. V. Efremov, S.-L. Drechsler, S. Aswartham, M. Kumar, S. Wurmehl, M. Roslova, I. V. Morozov, B. Holzapfel, B. Büchner, E. Ahrens, S. I. Troyanov, S. Köhler, E. Gati, S. Knöner, N. H. Hoang, M. Lang, F. Ricci, and G. Profeta, Phys. Rev. B **90**, 094511 (2014).
[44] S. L. Bud'ko, Y. Liu, T. A. Lograsso, and P. C. Canfield Phys. Rev. B **86**, 224514 (2012).
[45] C. P. Slichter, *Principles of Magnetic Resonance*, 3rd ed. (Springer, New York, 1990).
[46] K. Nishiyama, F. Dimmling, Th. Kornrumpf, and D. Riegel, Phys. Rev. Lett. **37** 357 (1976).
[47] S. L. Bud'ko, T. Kong , W. R. Meier, X. Ma and P. C. Canfield, Philosophical Magazine, **97**, 2689, (2017).
[48] J. Cui, Q.-P. Ding, W. R. Meier, A. E. Böhmer, T. Kong, V. Borisov, Y. Lee, S. L. Bud'ko, R. Valentí, P. C. Canfield, and Y. Furukawa, Phys. Rev. B **96**, 104512 (2017).
[49] Y. Kohori, Y. Yamato, Y. Iwamoto, T. Kohara, E. D. Bauer, M. B. Maple, and J. L. Sarrao, Phys. Rev. B **64**, 134526 (2001).
[50] T. Kohara, Y. Kohori, K. Asayama, Y. Kitaoka, M.B. Maple, and M. S. Torikachvili, Solid State Commun. **59**, 603 (1986).
[51] Y.-F. Yang, Z. Fisk, H.-O. Lee, J.D. Thompson, and D. Pines, Nature (London) **454**, 611 (2008).
[52] Z. T. Zhang, D. Dmytriieva, S. Molatta, J. Wosnitza, S. Khim, S. Gass, A.U.B. Wolter, S. Wurmehl, H.-J. Grafe, H. Kühne, arXiv:1703.00780.
[53] K. Kitagawa, N. Katayama, K. Ohgushi, and M. Takigawa, J. Phys. Soc. Jpn. **78**, 063706 (2009).
[54] S. Kitagawa, Y. Nakai, T. Iye, K. Ishida, Y. Kamihara, M. Hirano, and H. Hosono, Phys. Rev. B **81**, 212502 (2010).
[55] J. Li, D. Zhao, Y. P. Wu, S. J. Li, D. W. Song, L. X. Zheng, N. Z. Wang, X. G. Luo, Z. Sun, T. Wu, X. H. Chen, arXiv:1611.04694.
[56] R. E. Walstedt, *The NMR Probe of High-T_c Materials*, STMP 228 (Springer, Berlin Heidelberg 2008).
[57] K. Kitagawa, N. Katayama, H. Gotou, T. Yagi, K. Ohgushi, T. Matsumoto, Y. Uwatoko, and M. Takigawa, Phys. Rev. Lett. **103**, 257002 (2009).
[58] F. Hardy, T. Wolf, R. A. Fisher, R. Eder, P. Schweiss, P. Adelmann, H. v. Lhneysen, and C. Meingast, Phys. Rev. B **81**, 060501(R) (2010).
[59] L. P. Gor'kov and G. B. Teitel'baum, Phys. Rev. B **82**, 020510(R) (2010).
[60] Z. Shermadini, H. Luetkens, A. Maisuradze, R. Khasanov, Z. Bukowski, H.-H. Klauss, and A. Amato Phys. Rev. B **86** 174516 (2012).